

## Supporting Information

### Highly efficient photosynthesis of H<sub>2</sub>O<sub>2</sub> via two-channel pathway photocatalytic water splitting

Peipei Sun<sup>a</sup>, Zhao Mo<sup>a</sup>, Hanxiang Chen<sup>a</sup>, Yanhua Song<sup>b</sup>, Jinyuan Liu<sup>a</sup>, Weiqing Yin<sup>c</sup>,  
Hongliang Dai<sup>b</sup>, Zhigang Chen<sup>a,\*</sup>, Huaming Li<sup>a</sup>, Hui Xu<sup>a,\*</sup>

<sup>a</sup> School of the Environment and Safety Engineering, Institute for Energy Research, Jiangsu University, Zhenjiang 212013, P. R. China

<sup>b</sup> School of Environmental and Chemical Engineering, Jiangsu University of Science and Technology, Zhenjiang 212003, P. R. China

<sup>c</sup> Zhenjiang Environmental Monitoring Central Station, Zhenjiang 212009, P. R. China

\*Corresponding author e-mail address: chenzg@ujs.edu.cn, xh@ujs.edu.cn

## Table of Contents

### 1. Experimental

Characterization .....	3
Photocatalytic activity tests .....	3
Photoelectrochemical measurement.....	3
Transient photovoltage (TPV) measurements.....	4

### 2. Results and discussion

Fig. S1. EDX and SEM of CdS-0.....	5
Fig. S2. EDX and SEM of CdS-1.....	5
Fig. S3. N <sub>2</sub> adsorption-desorption isotherm of CdS-0 and CdS-1.....	6
Fig. S4. Contact angles of CdS-0 and CdS-1.....	6
Fig. S5. Images of dispersed catalysts in water with different treatment of CdS-0 and CdS-1.....	7
Fig. S6. The work curve of the concentration of H <sub>2</sub> O <sub>2</sub> and the absorption.....	7
Fig. S7. XRD; SEM image; N <sub>2</sub> adsorption-desorption isotherm and photocatalytic H <sub>2</sub> O <sub>2</sub> production of CdS-OH.....	8
Fig. S8. SEM and XRD pattern of CdS-1 after 3 cycles.....	8
Fig. S9. Comparison of the in-situ transient photovoltage with CdS-0 in different conditions.....	9
Table S1. Recent advances in photocatalysts for H <sub>2</sub> O <sub>2</sub> production.....	10
3. Reference.....	11

**Characterization:** TEM images were taken on a JEOL-JEM-2010 (JEOL, Japan) transmission electron microscope operated at 200 kV. The field emission scanning electron microscope (SEM) was JSM-7800F and equipped with an energy dispersive X-ray spectroscope. The powder X-ray diffraction (XRD) patterns were recorded by a Bruke D8 diffractometer with Cu K $\alpha$  radiation ( $\lambda = 1.5418 \text{ \AA}$ ) at a rate of  $7^\circ/\text{min}$ . The specific area was measured via Brunauer-Emmett-Teller (BET) method by N<sub>2</sub> adsorption-desorption isotherms (TriStar II 3020, Micromeritics Instrument Corporation, USA). X-ray photoelectron spectroscopy (XPS) analysis was collected on an ESCALab MKII X-ray photoelectron spectrometer using Mg K $\alpha$  radiation. Ultraviolet visible (UV-vis) diffuse reflection data were recorded using a UV-vis spectrophotometer (Shimadzu UV-3600 plus, Japan), and BaSO<sub>4</sub> was used as a reflectance standard material. The photoluminescence (PL) spectra were obtained by a QuantaMaster & TimeMaster Spectrofluorometer.

**Photocatalytic activity tests:** Photocatalytic H<sub>2</sub>O<sub>2</sub> production experiments were conducted with H<sub>2</sub>O, O<sub>2</sub>, and visible light irradiation at ambient temperature (25 °C). Exactly, 0.05 g of catalyst was suspended in 50 mL of distilled water in a glass reactor. Adsorption equilibrium was achieved following 30 min of stirring in the dark. Thereafter, the system was irradiated by visible light. 3mL of suspension was taken from reaction mixture and mixed with 0.75 mL of 0.4 M KI solution with 0.01 M ammonium molybdate and 0.75 mL of 0.1M C<sub>6</sub>H<sub>5</sub>KO<sub>4</sub> for 10 min. Absorbance was detected by UV-vis diffuse reflectance spectroscopy in 352nm. O<sub>2</sub> and N<sub>2</sub> was then bubbled into this system for 30 min to obtain an O<sub>2</sub>-equilibrated environment and N<sub>2</sub>-equilibrated environment.

**Photoelectrochemical measurement:** The photocurrents were measured by a CHI 660B electrochemical system, which was Equipped with a standard three-electrode system. 1 mg sample powder is dispersed ultrasonically in 1 mL deionized water, and 20  $\mu\text{L}$  of the resulting colloidal dispersion (1 mg/mL) is drop-cast onto a piece of ITO with a fixed area of 0.5 cm<sup>2</sup> and then dried under an infrared lamp to form the sample-modified ITO electrode. In the experiment, an ITO with a sample on it was used as a working electrode. Pt wire was employed as the counter electrode and the reference

electrode was Ag/AgCl/sat. KCl. A bias potential of -0.2 V (VS. Ag/AgCl) was employed. Na<sub>2</sub>SO<sub>4</sub> solution (0.1 M) was used as the electrolyte. The light source was a 500 W Xe lamp.

***Transient photovoltage (TPV) measurements:*** The TPV measurements were conducted at room temperature, including ex-situ and in-situ modes. In ex-situ mode, the platinum gage (1 cm×1 cm) with 20 mg sample was treated as the working electrode and Pt wires were used as the counter electrodes. In in-situ modes, working electrodes (1 cm×2 cm) were prepared by depositing samples (100 μL, 2 mg·mL<sup>-1</sup>) on indium-tin-oxide (ITO) glass substrates, then dried in air. During the testing process, the working electrodes were kept wet with N<sub>2</sub> saturated 1 vol% H<sub>2</sub>O/anhydrous acetonitrile aqueous (v/v) and N<sub>2</sub> or O<sub>2</sub> saturated anhydrous acetonitrile, respectively. These samples were excited by a laser radiation pulse ( $\lambda=355$  nm, pulse width 5 ns) from a third-harmonic Nd: YAG laser (Polaris II, New Wave Research, Inc.). The signal of the TPV was amplified by the amplifier and recorded by the oscilloscope.

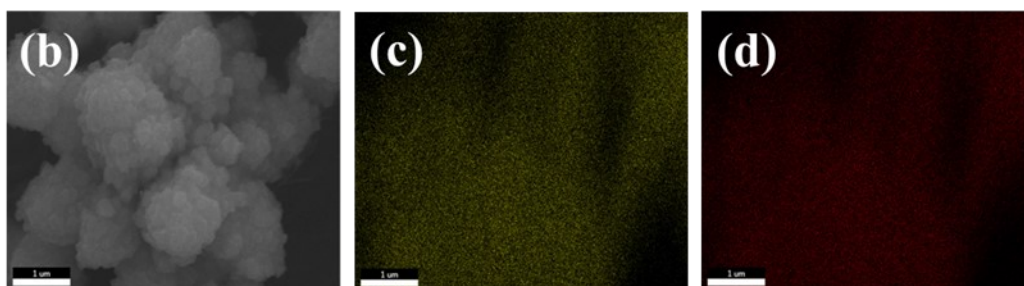
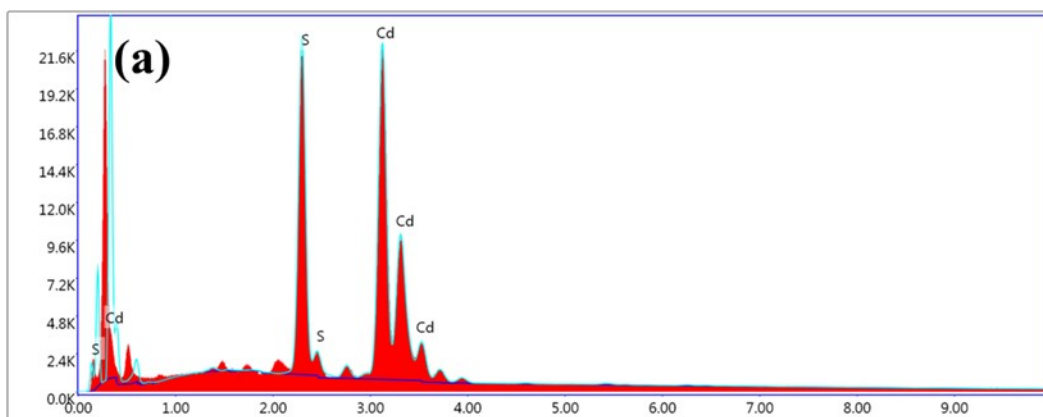


**Fig. S1.** (a) EDX spectra; (b) SEM image of CdS-0; (c-d) EDS elemental mappings for Cd and S corresponding to (b).

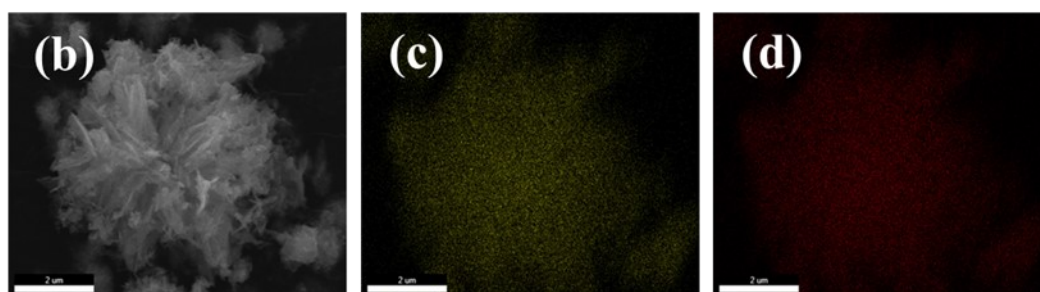
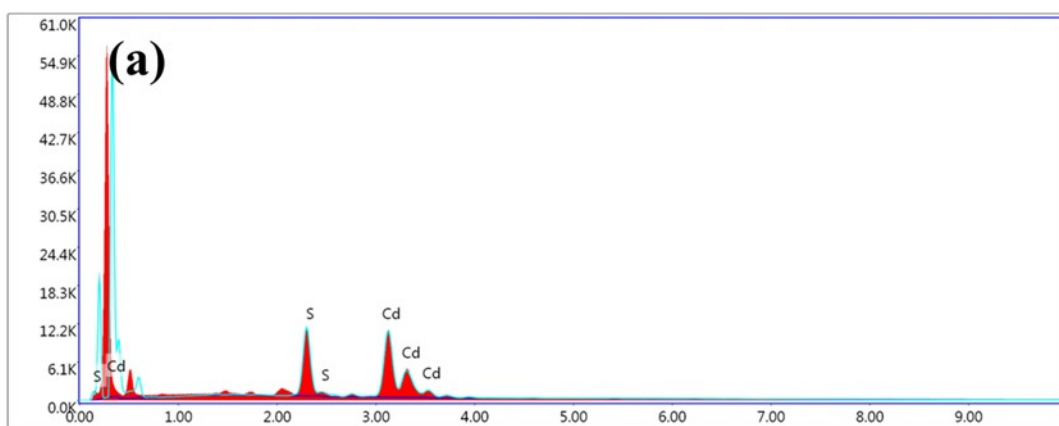


**Fig. S2.** (a) EDX spectra; (b) SEM image of CdS-1; (c-d) EDS elemental mappings for Cd and S corresponding to (b).

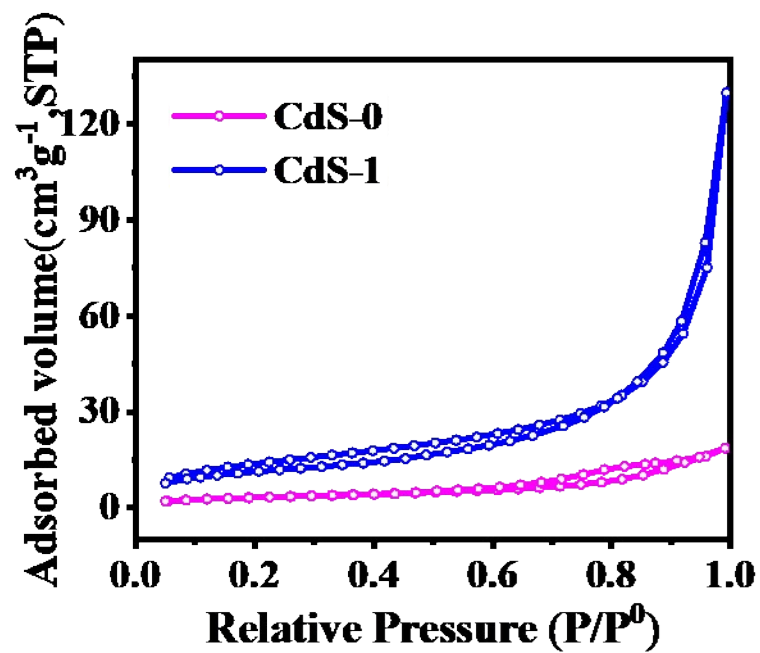


Fig. S3. N<sub>2</sub> adsorption-desorption isotherm of CdS-0 and CdS-1.

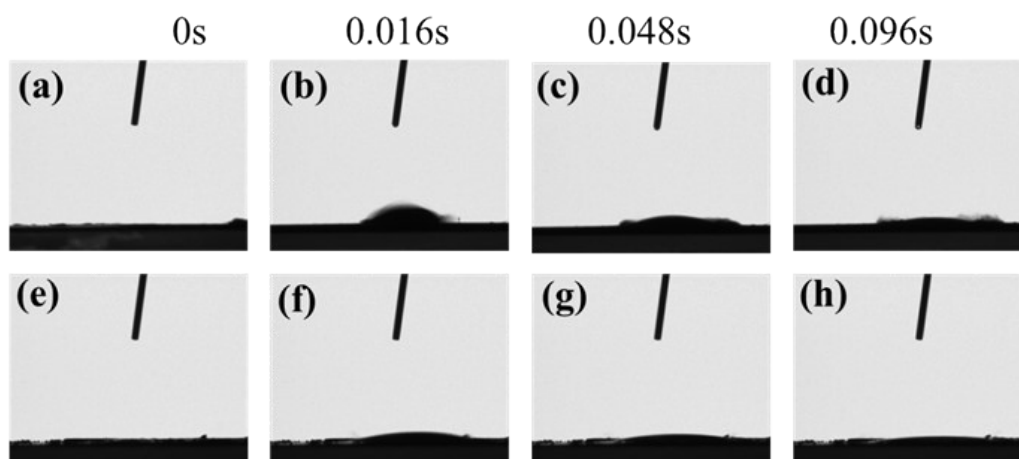


Fig. S4. Contact angles of CdS: (a–d) CdS-0; (e–h) CdS-1.

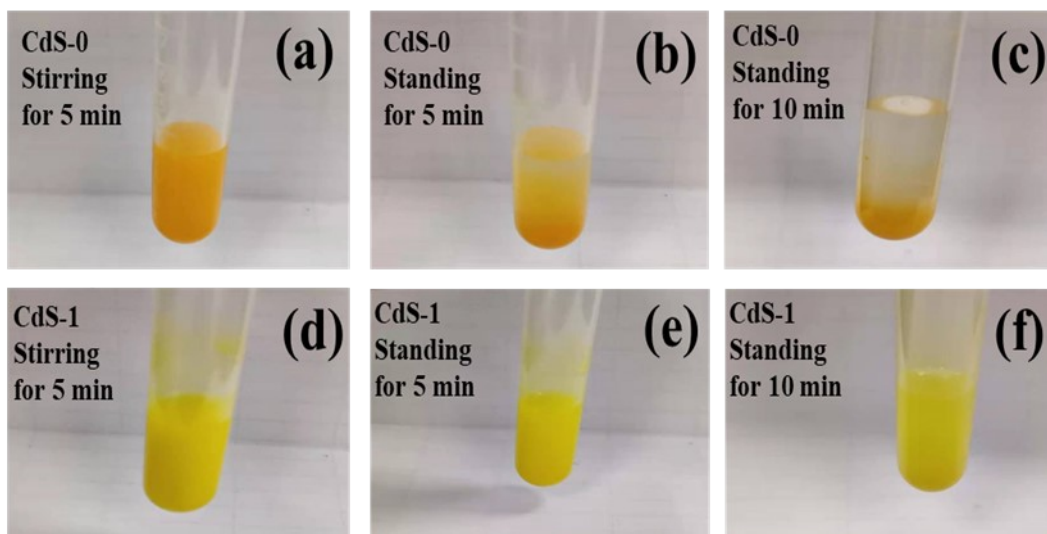


Fig. S5. Images of dispersed catalysts in water with different treatment: (a) CdS-0; (b) CdS-1.

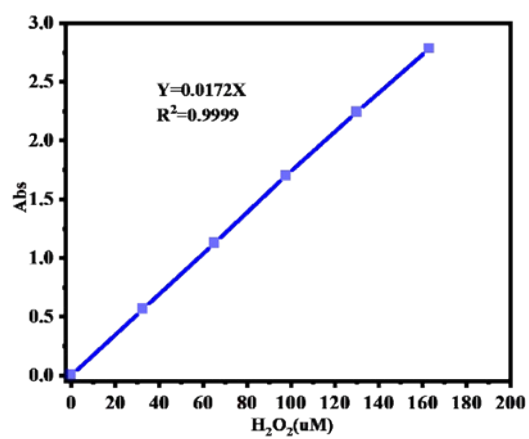


Fig. S6. The work curve of the concentration of H<sub>2</sub>O<sub>2</sub> and the absorption

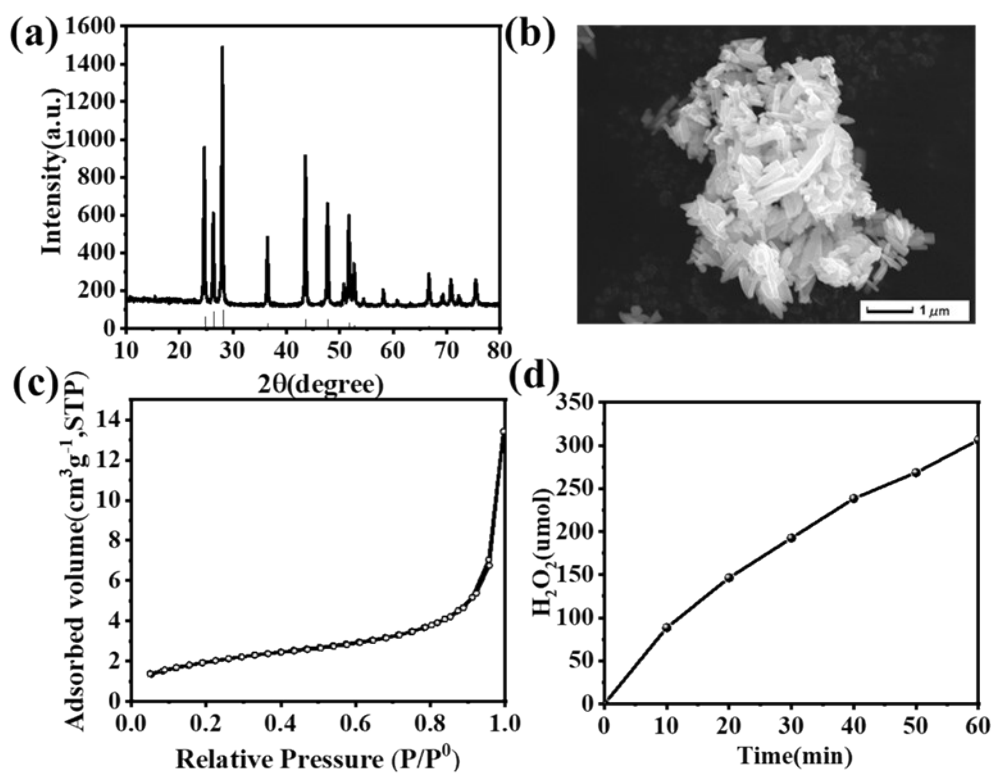


Fig. S7. (a) XRD; (b) SEM image; (c) N<sub>2</sub> adsorption-desorption isotherm; (d) Photocatalytic H<sub>2</sub>O<sub>2</sub> production of CdS-OH.

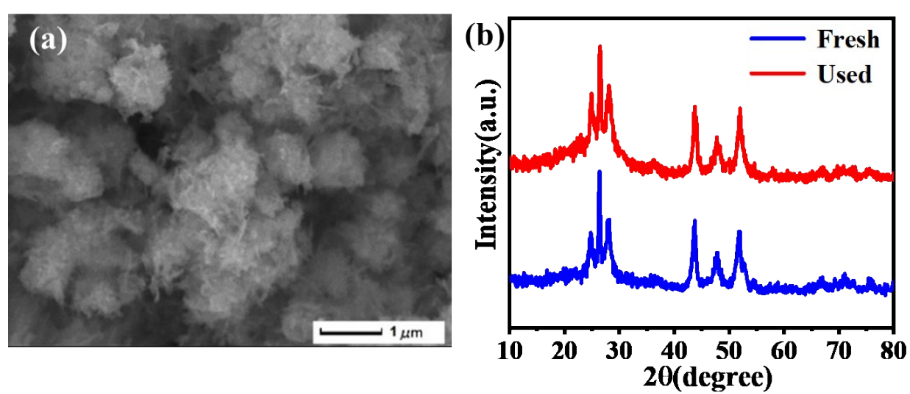


Fig. S8. (a) SEM image of CdS-1; (b) XRD pattern of CdS-1 after 3 cycles.

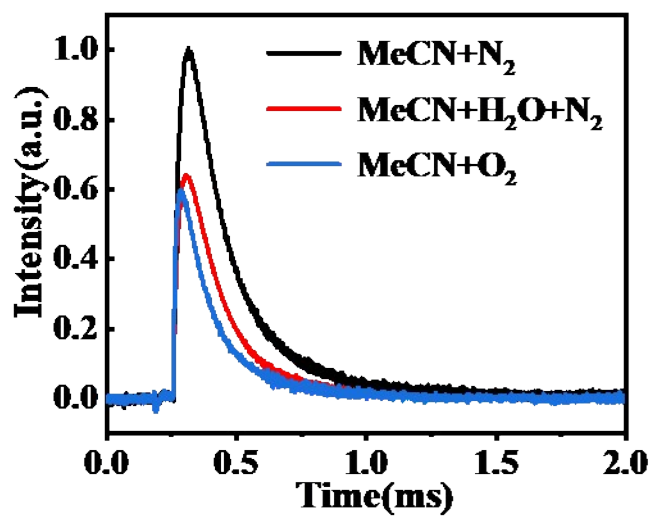


Fig. S9. Comparison of the in-situ transient photovoltage with CdS-0 in different conditions.

**Table S1.** Recent advances in photocatalysts for H<sub>2</sub>O<sub>2</sub> production

Catalyst	Light source	Reaction solution	H <sub>2</sub> O <sub>2</sub> production ( $\mu\text{mol h}^{-1} \text{g}^{-1}$ )	Ref.	<b>Ref ere nce</b>  [1] K ofuj i. Y. et al. AC S Cata l., Gra phiti c carb on niti de dop ed with biph enyl diim
g-C <sub>3</sub> N <sub>4</sub> /BDI <sub>51</sub>	$\lambda > 420 \text{ nm}$	1.67 g/L, O <sub>2</sub>	34	S1	
Au@MoS <sub>2</sub>	Sunlight	1.0 g/L, air, pH=9	91.67	S2	
PEI/C <sub>3</sub> N <sub>4</sub>	AM1.5, full arc	1.0 g/L, O <sub>2</sub>	208	S3	
g-C <sub>3</sub> N <sub>4</sub> /PDI <sub>51</sub>	$\lambda > 420 \text{ nm}$	1.67 g/L, O <sub>2</sub>	21	S4	
g-C <sub>3</sub> N <sub>4</sub> /PDI-rGO <sub>0.05</sub>	420nm< $\lambda$ <500 nm	1.67 g/L, O <sub>2</sub>	24	S5	
Mn <sub>3</sub> O <sub>4</sub> (20%)/Co <sub>9</sub> S <sub>8</sub>	300 W Xe, >420 nm	1.0 g/L, air	270	S6	
MMO@C <sub>3</sub> N <sub>4</sub>	300 W Xe	1.0 g/L, O <sub>2</sub> , pH=3	42	S7	
Cv-g-C <sub>3</sub> N <sub>4</sub>	300 W Xe, $\lambda > 420 \text{ nm}$	1.0 g/L, O <sub>2</sub>	100	S8	
ZnPPc-NBCN	$\lambda > 420 \text{ nm}$	0.5 g/L, air	114	S9	
g-C <sub>3</sub> N <sub>4</sub> /NaBH <sub>4</sub>	300 W Xe, >420 nm	1.0 g/L, air	170	S10	
CdS/rGO	$\lambda > 420 \text{ nm}$	1.0 g/L, O <sub>2</sub> , pH=5	213.3	S11	
g-C <sub>3</sub> N <sub>4</sub> /PI/rGO	$\lambda > 420 \text{ nm}$	1.0 g/L, air	950	S12	
CN/CuPO(20%)	Full-Spectrum	1.0 g/L, O <sub>2</sub>	1200	S13	
ZIF-8/C <sub>3</sub> N <sub>4</sub>	$\lambda > 420 \text{ nm}$	1.0 g/L, air	2641	S14	
CdS-0	$\lambda > 420 \text{ nm}$	1.0 g/L, air	184		
CdS-0.25	$\lambda > 420 \text{ nm}$	1.0 g/L, air Air	755.25		
CdS-0.33	$\lambda > 420 \text{ nm}$	1.0 g/L, air	789	This work	
CdS-0.67	$\lambda > 420 \text{ nm}$	1.0 g/L, air	1006.5		
CdS-0.75	$\lambda > 420 \text{ nm}$	1.0 g/L, air	1072.75		
CdS-1	$\lambda > 420 \text{ nm}$	1.0 g/L, air	1127.75		

ide: Efficient photocatalyst for hydrogen peroxide production from water and molecular oxygen by sunlight, 2016, 6, 7021-7029.

- [2] H. Song. et al. J. Catal., Photocatalytic production of H<sub>2</sub>O<sub>2</sub> and its in situ utilization over atomic-scale Au modified MoS<sub>2</sub> nanosheets, 2019, 376, 198-208.
- [3] X. K. Zeng. et al. ACS Catal., Simultaneously Tuning Charge Separation and Oxygen Reduction Pathway on Graphitic Carbon Nitride by Polyethylenimine for Boosted Photocatalytic Hydrogen Peroxide Production, 2020, 10, 3697-3706.
- [4] Shiraishi. Y. et al. Angew. Chem. Int. Ed., Sunlight-driven hydrogen peroxide production from water and molecular oxygen by metal-free photocatalysts, 2014,

- 53, 13454-13459.
- [5] Kofuji. Y. et al. *J. Am. Chem. Soc.*, Metal-Free photocatalysts for solar-to-hydrogen peroxide energy conversion with 0.2% efficiency, 2016, 138, 10019–10025.
- [6] H. Zhang. et al. *Appl. Catal. B: Environ.*, Photocatalytic production of hydrogen peroxide over Z-scheme  $\text{Mn}_3\text{O}_4/\text{Co}_9\text{S}_8$  with p-n heterostructure, 2021, 298, 120516.
- [7] R. Wang. et al. *ChemSusChem*, Solar-driven  $\text{H}_2\text{O}_2$  generation from  $\text{H}_2\text{O}$  and  $\text{O}_2$  using earth-abundant mixed-metal oxide@carbon nitride photocatalysts, 2016, 9, 2470–2479.
- [8] S. Li. et al. *Appl. Catal. B Environ.*, Effective photocatalytic  $\text{H}_2\text{O}_2$  production under visible light irradiation at g- $\text{C}_3\text{N}_4$  modulated by carbon vacancies, 2016, 190, 26–35.
- [9] Y. Ye. et al. *Proc. Natl. Acad. Sci. U.S.A.*, Highly efficient photosynthesis of hydrogen peroxide in ambient conditions, 2021, 118, e2103964118.
- [10] Z. Zhu. et al. *Appl. Catal. B: Environ.*, Visible light-driven photocatalytically active g- $\text{C}_3\text{N}_4$  material for enhanced generation of  $\text{H}_2\text{O}_2$ , 2018, 232, 19–25.
- [11] S. Thakur. et al. *J. Catal.*, Sunlight-driven sustainable production of hydrogen peroxide using a CdS–graphene hybrid photocatalyst, 2017, 345, 78-86.
- [12] L. Yang. et al. *Appl. Catal. B Environ.*, Engineering of reduced graphene oxide on nanosheet–g- $\text{C}_3\text{N}_4$ /perylene imide heterojunction for enhanced photocatalytic redox performance, 2019, 250, 42–51.
- [13] X. Wang. et al. *ACS Sustainable Chem. Eng.*, Synthesis of full-spectrum-response  $\text{Cu}_2(\text{OH})\text{PO}_4/\text{g}-\text{C}_3\text{N}_4$  photocatalyst with outstanding photocatalytic  $\text{H}_2\text{O}_2$  production performance via a “Two channel route”, 2018, 6, 14542–1455.
- [14] Y. J. Zhao. et al. *Appl. Catal. B-Environ.*, Efficient production of  $\text{H}_2\text{O}_2$  via two-channel pathway over ZIF-8/ $\text{C}_3\text{N}_4$  composite photocatalyst without any sacrificial agent, 2020, 278, 119289.